JCTC Journal of Chemical Theory and Computation

Combined QM/MM Molecular Dynamics Study on a Condensed-Phase S_N2 Reaction at Nitrogen: The Effect of Explicitly Including Solvent Polarization

Daan P. Geerke,[†] Stephan Thiel,[‡] Walter Thiel,[‡] and Wilfred F. van Gunsteren*[,†]

Laboratory of Physical Chemistry, Swiss Federal Institute of Technology Zürich, ETH, CH-8093 Zürich, Switzerland, and Max-Planck-Institut für Kohlenforschung, Kaiser-Wilhelm-Platz 1, D-45470 Mülheim, Germany

Received January 11, 2007

Abstract: In a previous combined QM/MM molecular dynamics (MD) study from our laboratory on the identity S_N2 reaction between a chloride anion and an amino chloride in liquid dimethyl ether (DME), an increase in the free energy activation barrier was observed in the condensed phase when compared to the gas-phase activation energy. Here we reproduce these findings, but when comparing the condensed-phase potential of mean force (PMF) with the *free* energy profile in the gas phase (obtained from Monte Carlo simulations), we observe a smaller solvent effect on the activation barrier of the reaction. In a next step, we introduce an explicit description of electronic polarization in the MM (solvent) part of the system. A polarizable force field for liquid DME was developed based on the charge-on-spring (COS) model, which was calibrated to reproduce thermodynamic properties of the nonpolarizable model in classical MD simulations. The COS model was implemented into the MNDO/GROMOS interface in a special version of the QM/MM software ChemShell, which was used to investigate the effect of solvent polarization on the free energy profile of the reaction under study. A higher activation barrier was obtained using the polarizable solvent model than with the nonpolarizable force field, due to a better solvation of and a stronger polarization of solvent molecules around the separate reactants. The obtained PMFs were subjected to an energy-entropy decomposition of the relative solvation free energies of the reactant complex along the reaction coordinate, to investigate in a quantitative manner whether the solvent (polarization) effects are mainly due to favorable QM-MM (energetic) interactions.

I. Introduction

In the present study, we use a combined QM/MM Hamiltonian[1−4] to extend a previous molecular dynamics (MD) study[5] of solvent effects on a S_N2 reaction at nitrogen in liquid dimethyl ether (DME). In combined QM/MM simulations, a small part of the system (the reactive subsystem) is treated quantum mechanically, whereas the rest of the system (the MM part) is described by a classical force field. The total combined Hamiltonian H consists of three terms[1−4]

$$H = H_{QM} + H_{QM/MM} + H_{MM} \quad (1)$$

H_{QM} and H_{MM} describe interactions within the QM and MM parts of the system, respectively. $H_{QM/MM}$ accounts for interactions between the QM and MM subsystems and is often described by an electrostatic coupling scheme[3,4,6−8] in which the field generated by the MM atoms is included in the QM Hamiltonian as a set of additional point-charges (first two terms on the right of eq 2). Other nonbonded interactions

* Corresponding author fax: (+41)-44-6321039; e-mail: wfvgn@igc.phys.chem.ethz.ch.
[†] Swiss Federal Institute of Technology Zürich.
[‡] Max-Planck-Institut für Kohlenforschung.

10.1021/ct7000123 CCC: $37.00
Published on Web 05/12/2007

between the QM and MM atoms are mimicked by adding the QM nuclei as van der Waals centers to the force field (last term on the right in eq 2). $H_{QM/MM}$ reads then as

$$H_{QM/MM} = -\sum_{i,m}\frac{q_m}{r_{im}} + \sum_{a,m}\frac{Z_a q_m}{r_{am}} + \sum_{a,m}\left(\frac{C_{12,a}^{1/2}C_{12,m}^{1/2}}{r_{am}^{12}} - \frac{C_{6,a}^{1/2}C_{6,m}^{1/2}}{r_{am}^{6}}\right) \quad (2)$$

in which the indices a and i run over the QM nuclei and electrons, respectively, and m runs over the MM atoms. Z and q are the (partial) charges of the QM nuclei and MM (united) atoms, respectively, and $C_{12}^{1/2}$ and $C_6^{1/2}$ are their repulsive and attractive Lennard-Jones parameters.

The reaction under investigation is the identity S_N2 reaction of a chloride anion with amino chloride

$$Cl^- + NH_2Cl \rightarrow ClNH_2 + Cl^- \quad (3)$$

The gas-phase potential energy surface (PES) for this reaction is characterized by a double-well potential, with a reactant or product ion-dipole complex (RC) located at the minima and a classical S_N2 transition state (TS) at the central barrier.[5,9] Liu et al.[5] showed that upon solvation in DME, the potential of mean force (PMF) for reaction 3 still has a double-well shape, but the free energy of formation of RC is less negative and the activation free energy barrier is more positive than the corresponding gas-phase energies. This can be explained from the distribution of the net negative charge over the reactive system, which is maximally concentrated on the nucleophile in the separated reactants. As a result, interactions with the polar DME liquid are stronger in the reactant state than for the RC and TS. Indeed, radial distribution functions for the solvent atoms around the nucleophile showed[5] a larger first solvation peak in the reactant state, indicating better solvation than in case of the complexes.

In the current study, we first repeated the QM/MM study on reaction 3 in DME. The reactive subsystem was described at the PM3 level of theory, which was shown by Liu[5] to be a valid choice. Like Liu, we use an electrostatic coupling scheme for the QM-MM interactions and a nonpolarizable DME force field. Thus, polarization of the electrons in the QM subsystem by the MM environment is automatically accounted for, but the solvent molecules cannot adapt their charge distribution in the course of the reaction. In addition we investigate the effect of taking solvent electron polarization into account on the PMF of reaction 3 from simulations using a combined QM/MM Hamiltonian with an explicit description of electron polarization effects in the MM part (designated as QM/MM-pol Hamiltonian). Because the net charge of the reactive subsystem varies from being concentrated on the nucleophile in the reactant state to being more spread out over the reactant complex and transition state, changes in the solvent molecular dipole moments along the reaction coordinate might well affect the reaction profile. Several MD studies[1,10−14] employed a QM/MM-pol Hamiltonian before, using either the induced point-dipole[1,15,16] or

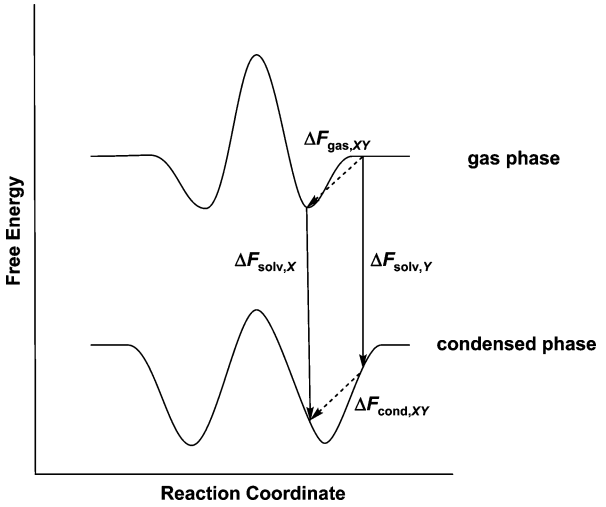

Figure 1. Schematic representation of the free energy profiles of a S_N2 reaction in the gas phase and in solution. The vertical arrows indicate the free energy of solvation ΔF_{solv} of the reactive complex at values for the reaction coordinate of X and Y, respectively. The dashed arrows are the relative free energy differences ΔF_{gas} and ΔF_{cond} along the reaction coordinate in the gas and condensed phase, respectively.

the fluctuating charge method[17,18] to account for electron polarization in the MM subsystem. Here we use the charge-on-spring (COS) model (or Drude-oscillator or shell model)[19−21] to describe the MM inducible dipoles. An attractive feature of the COS method for use in QM/MM simulations is that the induced dipoles directly enter $H_{QM/MM}$ via additional point charges in eq 2. For our QM/MM-pol simulations, a COS-based model for DME was parametrized based on the nonpolarizable force field, and the Charge-on-Spring model was implemented into a special version[22] of the GROMOS96 software[23,24] interfaced to the ChemShell QM/MM software package.[8]

Liu studied solvent effects on reaction 3 from a comparison between the condensed-phase *free* energy profile (PMF) and the gas-phase *potential* energy surface (PES). To obtain a more complete picture of the solvent effects, we also consider differences with the gas-phase *free* energy profile along the reaction coordinate. Once the free energy profiles in vacuum and the solvent are known, a direct quantitative measure for the solvent effect on the reaction profile can be obtained by defining the relative difference in the "free energy of solvation" of the reactive subsystem ($\Delta\Delta F_{solv}$) along the reaction coordinate rc

$$\Delta\Delta F_{solv,XY} = \Delta F_{solv,X} - \Delta F_{solv,Y} \quad (4)$$

with $\Delta F_{solv,X}$ and $\Delta F_{solv,Y}$ the free energy change upon transferring the reactive subsystem from vacuum into the liquid at values X and Y for rc, respectively. Values for $\Delta\Delta F_{solv}$ can also be calculated from applying a thermodynamic cycle (see Figure 1)

$$\Delta\Delta F_{solv,XY} = \Delta F_{cond,XY} - \Delta F_{gas,XY} \quad (5)$$

with $\Delta F_{cond,XY}$ and $\Delta F_{gas,XY}$ being the condensed-phase and gas-phase free energy difference along the reaction coordinate when going from rc = Y to rc = X, respectively.

Liu's finding that better solvation of the charge-localized reactants is responsible for the increase in the barrier height when compared to the gas-phase PES hints at energetic interactions determining the solvent effect. In an attempt to quantify whether this is the case, we apply an energy-entropy decomposition scheme for solvation free energies ΔF_{solv}, which has recently successfully been applied to study driving forces behind hydrophobic solvation and cosolvent interactions in aqueous mixtures.[25−29] Starting point of this decomposition scheme is to separate ΔF_{solv} (corresponding with the free energy change of bringing a solute molecule (indicated by the index "u") from vacuum into a solvent (indicated by the index "v")) into energy and entropy contributions from solute−solute (uu), solute−solvent (uv), and solvent−solvent (vv) interactions

$$\begin{aligned}\Delta F_{\mathrm{solv}} &= \Delta U - T\Delta S \\ &= \Delta U_{\mathrm{uu}} + \Delta U_{\mathrm{uv}} + \Delta U_{\mathrm{vv}} \\ &\quad - (T\Delta S_{\mathrm{uu}} + T\Delta S_{\mathrm{uv}} + T\Delta S_{\mathrm{vv}})\end{aligned} \tag{6}$$

From statistical mechanics, it can be shown that the energy and entropy terms arising from solvent−solvent interactions exactly cancel out,[30] that is

$$\Delta U_{\mathrm{vv}} = T\Delta S_{\mathrm{vv}} \tag{7}$$

Here, we include solute−solute energies and entropies of solvation into the corresponding solute−solvent terms, which reduces eq 6 to

$$\Delta F_{\mathrm{solv}} = \Delta U_{\mathrm{uv}} - T\Delta S_{\mathrm{uv}} \tag{8}$$

Thus, ΔU_{uv} (accounting for energetic interactions between the solute and solvent) and ΔS_{uv} (a measure for the probability for the solvent to open up solute-sized cavities and to undergo favorable interactions with the solute) are the terms to analyze to understand trends in ΔF_{solv} at a microscopic level.[25−29]

Here, we consider the reactive subsystem as the solute and monitor relative differences in its free energy of solvation along a reaction coordinate rc (see Figure 1). Using eq 4, $\Delta\Delta F_{\mathrm{solv},XY}$ (the relative difference in ΔF_{solv} in going from an rc value of Y to X) reads then

$$\begin{aligned}\Delta\Delta F_{\mathrm{solv},XY} &= \Delta F_{\mathrm{solv},X} - \Delta F_{\mathrm{solv},Y} \\ &= \Delta U_{\mathrm{uv},X} - T\Delta S_{\mathrm{uv},X} - (\Delta U_{\mathrm{uv},Y} - T\Delta S_{\mathrm{uv},Y}) \\ &= \Delta\Delta U_{\mathrm{uv},XY} - T\Delta\Delta S_{\mathrm{uv},XY}\end{aligned} \tag{9}$$

where $\Delta\Delta U_{\mathrm{uv},XY}$ and $T\Delta\Delta S_{\mathrm{uv},XY}$ are the relative differences in ΔU_{uv} and $T\Delta S_{\mathrm{uv}}$ between rc values of X and Y, respectively. Here, $\Delta\Delta U_{\mathrm{uv},XY}$ is simply the corresponding difference in solute−solvent (QM-MM) interaction energy, corrected by the solute−solute (QM) reorganization energy

$$\begin{aligned}\Delta\Delta U_{\mathrm{uv},XY} &= \Delta U_{\mathrm{uv},X} - \Delta U_{\mathrm{uv},Y} \\ &= \hat{H}_{\mathrm{QM/MM},X} + \hat{H}_{\mathrm{QM,liq},X} - \hat{H}_{\mathrm{QM,gas},X} \\ &\quad - (\hat{H}_{\mathrm{QM/MM},Y} + \hat{H}_{\mathrm{QM,liq},Y} - \hat{H}_{\mathrm{QM,gas},Y})\end{aligned} \tag{10}$$

and

$$T\Delta\Delta S_{\mathrm{uv},XY} = \Delta\Delta U_{\mathrm{uv},XY} - \Delta\Delta F_{\mathrm{solv},XY} \tag{11}$$

In the QM/MM-pol simulations, changes in the self-polarization energy of the solvent molecules along the reaction coordinate (ΔU_{self}) are included in $\Delta\Delta U_{\mathrm{uv}}$ (because U_{self} accounts for the cost of the change in polarization of the solvent molecules due to a change in the value of rc), and eq 10 reads

$$\begin{aligned}\Delta\Delta U_{\mathrm{uv},XY} &= \hat{H}_{\mathrm{QM/MM},X} + \hat{H}_{\mathrm{QM,liq},X} - \hat{H}_{\mathrm{QM,gas},X} \\ &\quad - (\hat{H}_{\mathrm{QM/MM},Y} + \hat{H}_{\mathrm{QM,liq},Y} - \hat{H}_{\mathrm{QM,gas},Y}) \\ &\quad + \Delta U_{\mathrm{self},XY}\end{aligned} \tag{12}$$

where

$$\Delta U_{\mathrm{self},XY} = U_{\mathrm{self},X} - U_{\mathrm{self},Y} \tag{13}$$

From trends in $\Delta\Delta U_{\mathrm{uv}}$ and $T\Delta\Delta S_{\mathrm{uv}}$ we analyze the origin of free energy differences along the reaction coordinate and, hence, the solvent (polarization) effect on reaction 3 in DME.

II. The Charge-on-Spring Model To Account for Electron Polarization in the MM Subsystem

Following the charge-on-spring (COS) model,[21,22,31] the MM inducible dipoles are represented by an additional massless site with a point charge $q_{\mathrm{pol},i}$ attached to the polarizable MM centers i (having a charge of $q_i - q_{\mathrm{pol},i}$), via a spring with a force constant depending on its polarizability α_i. The induced dipoles $\vec{\mu}_{\mathrm{ind},i}$ are then represented by a displacement $\Delta\vec{r}_{\mathrm{pol},i}$ of the spring

$$\vec{\mu}_{\mathrm{ind},i} = q_{\mathrm{pol},i}\Delta\vec{r}_{\mathrm{pol},i} \tag{14}$$

For a given configuration of QM and MM atoms, the QM wavefunction is optimized in an SCF calculation in which the wavefunction 'feels' the MM polarization by including the charges-on-spring and their (fixed) positions in the first two terms in eq 2. Subsequently, the displacements $\Delta\vec{r}_{\mathrm{pol},i}$ of the charges-on-spring attached to the MM polarizable centers are calculated as

$$\Delta\vec{r}_{\mathrm{pol},i} = \frac{\alpha_i(4\pi\epsilon_0)\vec{E}_i}{q_{\mathrm{pol},i}} \tag{15}$$

where $\vec{E}_i$ is the electric field at center i and is calculated as the sum of the contributions from the MM nuclei and charges-on-spring (see eq 59 in ref 31) and from the (fixed) QM wavefunction (determined from the QM gradients at i). Because the $\vec{E}_i$'s depend on the positions of all other charges-on-spring, the $\vec{\mu}_{\mathrm{ind},i}$'s ($\Delta\vec{r}_{\mathrm{pol},i}$'s) in the MM subsystem are determined in an iterative way, until the induced dipole interaction energies are converged. Thus, a doubly iterative scheme has to be employed: since the polarization of the QM electrons and MM polarizable centers affect each other, iterations over the QM and MM SCF procedures are performed until the total QM/MM-pol energy is converged. To ensure full convergence of the QM electron wavefunction,

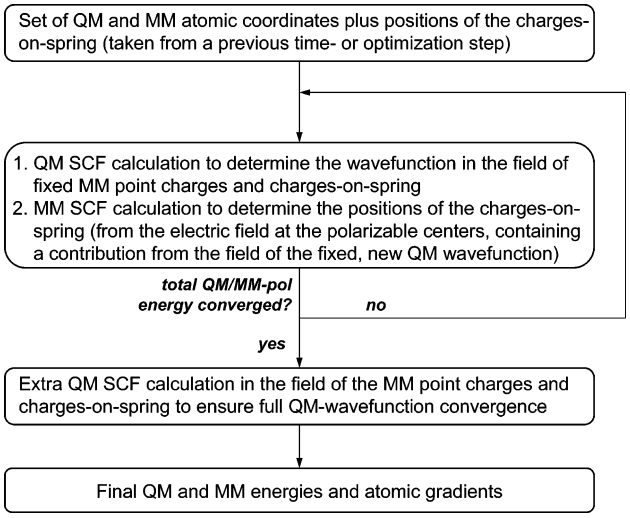

Figure 2. Schematic representation of the SCF procedure to determine the total QM/MM-pol energy and the gradients on the QM and MM nuclei for a set of atomic positions, as implemented in a special version of the GROMOS interface to ChemShell that is adapted to the charge-on-spring model.

an additional QM SCF calculation is performed after the last QM/MM iteration step. This procedure is summarized in Figure 2. The total forces on the MM polarizable centers for the use in the next MD or geometry optimization step are calculated by adding the contributions from the electrostatic gradients on the massless charges-on-spring to the forces acting on the atom they are attached to.[21,22] Additionally to the extra point charges (the charges-on-spring) that enter H_{MM} and $H_{QM/MM}$, a self-polarization energy term (U_{self}) is to be added to the QM/MM-pol Hamiltonian to account for the energy cost of inducing the dipoles[32]

$$U_{self} = \frac{1}{2}\sum_i \frac{\vec{\mu}_{ind,i}\cdot\vec{\mu}_{ind,i}}{\alpha_i(4\pi\epsilon_0)} = \frac{1}{2}\sum_i \frac{q_{pol,i}^{\ 2}|\Delta\vec{r}_{pol,i}|^2}{\alpha_i(4\pi\epsilon_0)} \quad (16)$$

U_{self} is a direct measure of the contribution from the induced dipoles to the total energy of the system, since it is the negative of this contribution.[32]

III. Simulation Setup

Potential energy surfaces (PES) and potentials of mean force (PMF) for reaction 3 were obtained along a reaction coordinate rc defined in terms of the bond distances of the incoming and the leaving chloride anion to the central nitrogen, r_{N-Cl1} and r_{N-Cl2}, respectively

$$rc = r_{N-Cl1} - r_{N-Cl2} \quad (17)$$

with rc = 0.0 nm corresponding to the transition state and rc adopting an infinite value for the separate reactants. The gas-phase PES was obtained from energy minimizations (using the hdlcopt geometry optimizer[33] implemented in ChemShell[8]) in which values for rc were kept fixed and gradually increased in steps of 0.01 nm starting from rc = 0.0 nm (the transition state) until an energy plateau was reached. The PMF in vacuum was obtained from a series of Monte Carlo (MC) simulations at 248.15 K, in which a harmonic potential-energy function was employed to keep rc close to a target value rc_{target} (varied from 0.0 to 1.1 nm with increments of 0.01 nm)

$$V_{umb} = \frac{1}{2}k_{umb}(rc - rc_{target})^2 \quad (18)$$

The force constant k_{umb} was set to a large value ($6 * 10^6$ kJ mol^{-1} nm^{-2}) to ensure narrow distributions of rc values around rc_{target}. In every MC simulation, 10^6 trial steps were performed (after 1000 steps of equilibration) in which the Cartesian coordinates of one of the atoms were varied with a maximum random displacement of 10^{-3} nm. Gas-phase energies and gradients were calculated at the PM3 level of theory using the MNDO99 code[34] interfaced to ChemShell.

In the combined QM/MM simulations of reaction 3 in liquid dimethyl ether (DME), the reactive subsystem was described by the PM3 Hamiltonian and the solvent by either a nonpolarizable (DME_{nonpol}) or a polarizable force field (DME_{pol}). Parameters for the (rigid, united-atom) DME_{nonpol} model were taken from Liu et al.,[5] see Table 1. The DME_{pol} model was developed based on DME_{nonpol} using the charge-on-spring (COS) method.[19−21] Massless sites with a charge of $q_{pol} = -8.0\ e$ were attached to DME's atomic centers. The polarizabilities α_i for O and CH_3 were taken from Miller,[35] where α_i of the CH_3 group was calculated as the sum of the polarizabilities of the atoms it is composed of. The nonbonded parameters were adapted to obtain a model that reproduces the density and heat of vaporization of the DME_{nonpol} model in MD simulations of the pure liquid under NpT boundary conditions. The rationale was to lower the Lennard-Jones well depth of one of the atom types (the oxygen) in the DME_{pol} model, since this parameter effectively accounts for polarization effects in nonpolarizable force fields. For the simulations of the DME_{nonpol} liquid, the GROMOS96 simulation package[23,24] was used, and for the DME_{pol} simulations an adapted version[22] of this package was used. Temperature and pressure were kept constant at 248.15 K and 1 atm using the weak-coupling approach[36] with coupling times of 0.1 and 0.5 ps, respectively, and an isothermal compressibility of $4.575*10^{-4}$ (kJ mol^{-1} nm^{-3})$^{-1}$ for the pressure bath. Bond lengths were kept fixed using the SHAKE procedure[37] with a relative geometric accuracy of 10^{-4}. The time step was 2 fs. A triple-range cutoff scheme was applied: nonbonded interactions within 0.8 nm were calculated every step from a charge-group based pairlist that was updated every five steps. At these time points, interactions between 0.8 and 1.4 nm were calculated and kept constant between updates. A reaction-field contribution[38] was added to the electrostatic interactions and forces, in which the dielectric permittivity was set to 4. The system consisted of 512 molecules which were initially placed in a random orientation in a cubic box at the experimental density[39] of 737 kg m^{-3}. After an initial energy minimization, the system was equilibrated for 20 ps and simulated for an additional 200 ps in which data were saved every 100 steps for analysis. The density and heat of vaporization of the liquid were calculated, as well as its static dielectric permittivity which was calculated from fluctuations in the total dipole moment of

Table 1. Nonpolarizable (DME_{nonpol})[5] and Polarizable (DME_{pol}) Force-Field Parameter Sets for the Rigid United-Atom Models for Liquid Dimethyl Ether and van der Waals Parameters[5] for the QM Subsystem (NH_2Cl_2)

parameter[a]	DME_{nonpol}	DME_{pol}	parameter[a]	NH_2Cl_2
r_{O-CH3} [nm]	0.141	0.141		
$r_{CH3-CH3}$ [nm]	0.2324	0.2324		
q_O [e]	−0.36	−0.36		
q_{CH3} [e]	0.18	0.18		
$C_6^{1/2}$ (O) [kJ mol^{-1} nm^6]$^{1/2}$	0.04756	0.042663	$C_6^{1/2}$ (N) [kJ mol^{-1} nm^6]$^{1/2}$	0.04936
$C_{12}^{1/2}$ (O) [10^{-3} (kJ mol^{-1} nm^{12})^{12}]	0.86115	0.7761	$C_{12}^{1/2}$ (N) [10^{-3} (kJ mol^{-1} nm^{12})^{12}]	1.301
$C_6^{1/2}$ (CH_3) [kJ mol^{-1} nm^6]$^{1/2}$	0.09421	0.09421	$C_6^{1/2}$ (Cl) [kJ mol^{-1} nm^6]$^{1/2}$	0.1175
$C_{12}^{1/2}$ (CH_3) [10^{-3} (kJ mol^{-1} nm^{12})^{12}]	5.1137	5.1137	$C_{12}^{1/2}$ (Cl) [10^{-3} (kJ mol^{-1} nm^{12})^{12}]	10.34
α_O [10^{-3} nm^3]		0.637	$C_6^{1/2}$ (H) [kJ mol^{-1} nm^6]$^{1/2}$	0.0
α_{CH3} [10^{-3} nm^3]		2.222	$C_{12}^{1/2}$ (H) [10^{-3} (kJ mol^{-1} nm^{12})^{12}]	0.0

[a] r_{O-CH3} and $r_{CH3-CH3}$: $O-CH_3$ and CH_3-CH_3 bond lengths corresponding with a CH_3-O-CH_3 angle of 111.0 degrees for both models. *q:* partial charges, $C_6^{1/2}$ and $C_{12}^{1/2}$: attractive and repulsive van der Waals parameters, and α: atomic polarizability.

the simulation box, according to a Kirkwood-Fröhlich type equation derived by Neumann.[22,40]

In the QM/MM simulations, interactions between the QM and MM subsystems were treated using an electrostatic coupling scheme (eq 2), and van der Waals parameters for the QM atoms are given in Table 1. Energy and gradient evaluations for the QM and MM regions were performed by the MNDO99[34] and GROMOS96[23,24] codes, respectively, interfaced to ChemShell.[8] For the energy and gradient evaluations in the QM/MM-pol simulations, a doubly iterative scheme (Figure 2) was implemented in the ChemShell interface, using a special version of the GROMOS96 code adapted to the COS model.[22] For every configuration of atomic positions, a fixed number of QM/MM SCF iterations was performed, starting with the COS displacements $\Delta\vec{r}_{pol,i}$ as determined in the previous time or optimization step. The number of iterations was set to 4, which was found to be large enough to achieve an energy convergence of the total QM/MM-pol Hamiltonian within 0.025 kJ mol^{-1}. Energy convergence criteria for the separate QM and MM SCF calculations were set to 10^{-8} eV and 10^{-3} kJ mol^{-1}, respectively.

Molecular dynamics simulations of reaction 3 in liquid DME under NVT conditions were performed using the dynamics routine of ChemShell,[8] with a time step of 0.5 fs. The temperature was kept constant at 248.15 K using a Berendsen thermostat[36] with a coupling time of 0.1 ps. Geometries of the solvent molecules were kept rigid by constraining bond lengths using the SHAKE algorithm[37] with a relative geometric accuracy of 10^{-8}. For the QM-MM interactions, a straight cutoff truncation scheme was applied. Interactions between the QM subsystem and DME solvent molecules were taken into account if the position of the DME molecule's center of geometry is within 1.1 nm of any of the QM atoms. For the MM−MM interactions, a twin-range cutoff was applied using a charge-group based pairlist which was updated every 5 steps: interactions between molecules with the distance between the center of geometries of less than 0.8 nm were calculated explicitly every step and between 0.8 and 1.1 nm every fifth step.

The free energy profile in DME was obtained from a series of QM/MM MD simulations at different values for rc in which its value was constrained to a target value rc_{target} using the SHAKE procedure.[37,41] Simulations were performed at 63 different values for rc_{target}: between values of 0−0.04 nm, rc_{target} was incremented in steps of 0.004 nm; between 0.04 and 0.2 nm, rc_{target} was incremented in steps of 0.005 nm; and between 0.2 and 0.4 nm, rc_{target} was incremented in steps of 0.01 nm. Initial coordinates for the simulations were generated as follows. First, the gas-phase optimized geometry of the transition state was placed in the center of a cubic box which was filled by adding 350 DME molecules in a random orientation. The box volume (35.8929 nm^3) was chosen such that the density of the solvent was equal to the density of the liquid model. After an energy minimization, initial atomic velocities were assigned from a random Maxwell−Boltzmann distribution corresponding to a temperature of 248.15 K, and a series of equilibration runs was performed with increasing values of rc_{target} (starting from 0.0 nm). Every equilibration run of 5 ps started with the final set of atomic positions and velocities from the previous simulation. In the initial geometry optimization and equilibration runs, the DME_{nonpol} model was used. The final configurations of the equilibration runs were used as starting configurations for the production runs using the nonpolarizable force field and for additional equilibration runs of 4 ps using the DME_{pol} model to generate starting structures for the production runs with the QM/MM-pol Hamiltonian. All production runs had a length of 20 ps. Constrained forces, energies, QM charge distributions, and positions of the MM atoms and charges-on-spring were saved every 100 step for analysis. To check for inaccuracies in the condensed-phase PMF due to hysteresis, we additionally performed the same sets of QM/MM simulations but starting from rc = 0.4 nm in the equilibration procedure: the separated reactants were solved in DME, and rc was gradually decreased (in steps of 0.01 nm) to rc = 0.0 nm in the equilibration simulations using the DME_{nonpol} model. In this way, starting structures for the production runs and for the QM/MM-pol equilibration runs were obtained.

Free energy differences along the reaction coordinate were calculated using the thermodynamic integration formalism:[42] identifying ξ with the reaction coordinate, the free energy difference $\Delta F_{a\rightarrow b}$ between two values a and b for ξ is evaluated as the potential of mean force of constraint[43−45]

$$\Delta F_{a\rightarrow b} = \int_a^b \mathrm{d}\xi \left\langle \frac{\partial V}{\partial \xi} \right\rangle_\xi \qquad (19)$$

where $\langle \partial V/\partial \xi \rangle_\xi$ is the force of constraint along the reaction coordinate, defined as the derivative of the potential energy V of the system with respect to ξ. In the vacuum simulations, this force was directly calculated from the average value of the umbrella force[46] at every MC step. In the condensed-phase simulations, it was evaluated as the average of the difference between unconstrained and constrained forces.[41] The use of a constraint on a reaction coordinate results in the introduction of a metric tensor effect,[43,47−51] which in the case of a reaction coordinate as defined in eq 17 can be corrected for by adding a term to eq 19 after which the expression for $\Delta F_{a\rightarrow b}$ reads as

$$\Delta F_{a\rightarrow b} = \int_a^b \mathrm{d}\xi \left\langle \frac{\partial V}{\partial \xi} \right\rangle_\xi - k_\mathrm{B}T \ln \frac{\langle z^{-1/2} \rangle_{\xi=b}}{\langle z^{-1/2} \rangle_{\xi=a}} \qquad (20)$$

with

$$z = m_{\mathrm{Cl1}}{}^{-1} + 2m_{\mathrm{N}}{}^{-1}(1 + \cos(\vec{r}_{\mathrm{N-Cl1}}, \vec{r}_{\mathrm{N-Cl2}})) + m_{\mathrm{Cl2}}{}^{-1} \qquad (21)$$

where $\cos(\vec{r}_{\mathrm{N-Cl1}}, \vec{r}_{\mathrm{N-Cl2}})$ is the cosine of the angle between the $\mathrm{N-Cl_1}$ and $\mathrm{N-Cl_2}$ (bond) vectors, and the m_i's are the masses of the atoms. The integral in eq 19 was evaluated via trapezoidal integration. Errors in energy values and the constrained and restrained forces were estimated at every rc value using the block-averaging procedure described by Allen and Tildesley.[52] Individual errors in the forces were integrated to yield the total error in the free energy differences along the reaction coordinate.

Free energies of solvation (ΔF_{solv}) in nonpolarizable DME were calculated for the transition state and the separated reactants. Three sets of simulations were performed: one for the complete QM subsystem in which rc was kept constrained at 0.0 nm (transition state). For the reactants, two separate sets of simulations of NH_2Cl and Cl^- in $\mathrm{DME_{nonpol}}$ were performed. In all three cases, two subsets of simulations were performed: first, electrostatic interactions between the QM and MM subsystems were gradually turned off using a coupling parameter λ that linearly scales down QM-MM electrostatic interactions (with $\lambda = 1$ corresponding to full and $\lambda = 0$ corresponding to no interactions). Subsequently a set of simulations was performed in which QM-MM van der Waals interactions were linearly scaled down from $\lambda = 1$ to $\lambda = 0$. Simulations were performed at 21 evenly distributed λ-points, with 5 ps equilibration and 20 ps of production per λ-point. At every λ-point, the free energy change in going from the actual value λ_a to $\lambda_\mathrm{b} = \lambda_\mathrm{a} - 0.05$, was calculated using perturbation theory[53]

$$\Delta F_{\lambda_a\rightarrow\lambda_b} = -k_\mathrm{B}T \ln \langle e^{-(H(\lambda_b)-H(\lambda_a))/k_\mathrm{B}T} \rangle_{\lambda_a} \qquad (22)$$

with $H(\lambda_x)$ being the total potential energy of the system calculated with the Hamiltonian corresponding to λ_x from configurations saved every 100 steps during the production runs. ΔF_{solv} was obtained as minus the total sum of the values for $\Delta F_{\lambda_a\rightarrow\lambda_b}$ (corresponding to the free energy of turning off electrostatic and van der Waals QM-MM interactions, respectively) calculated at $\lambda_\mathrm{a} = 1, 0.95, ..., 0.05$.

IV. Results and Discussion

IV.1. Parametrization of a Polarizable Force Field for Liquid Dimethyl Ether. The optimized polarizable parameter set for liquid dimethyl ether (DME) is given in Table 1 and reproduces the density and heat of vaporization of the nonpolarizable $\mathrm{DME_{nonpol}}$ model within 1%, see Table 2. Note that $\mathrm{DME_{nonpol}}$ slightly overestimates the experimental density (737 kg $\mathrm{m^{-3}}$)[39] and underestimates the experimental heat of vaporization (21.7 kJ $\mathrm{mol^{-1}}$),[54] see Table 2. However, the goal is to parametrize a polarizable model which is as close as possible to $\mathrm{DME_{nonpol}}$, in order to get a clear picture of the effect of treating solvent polarization effects explicitly in the study of reaction 3 in DME. The self-polarization energy (U_{self}) contribution to the total potential energy of the polarizable model ($\mathrm{DME_{pol}}$) is only 5%, see Table 2. However, polarization effects will play a more important role in heterogeneous, more polar (ionic) media, as shown below for the case of a changing charge distribution over the solute system along the reaction coordinate. The static relative dielectric permittivities of the $\mathrm{DME_{nonpol}}$ and $\mathrm{DME_{pol}}$ models are also given in Table 2, with the permittivity being significantly higher for the latter one (6.8 versus 4.7). We could not find experimental data to compare these values with, and for this system of relatively low dielectric permittivity, 200 ps of simulation was enough to obtain convergence.

Table 2. Thermodynamic and Dielectric Properties for Liquid Dimethyl Ether at 248.15 K and 1 atm from Experiment and from MD Simulations Using the Nonpolarizable Force Field ($\mathrm{DME_{nonpol}}$)[5] and the Polarizable Model ($\mathrm{DME_{pol}}$) Developed in the Current Work

property[a]	experiment	$\mathrm{DME_{nonpol}}$	$\mathrm{DME_{pol}}$
T [K]	248.15	248.0	248.0
ρ [kg $\mathrm{m^{-3}}$]	737[b]	751	749
ΔH_{vap} [kJ $\mathrm{mol^{-1}}$]	21.7[c]	21.3	21.1
$-U_{\mathrm{pot}}$ [kJ $\mathrm{mol^{-1}}$]		19.2	20.1
U_{self} [kJ $\mathrm{mol^{-1}}$]			1.1
ϵ		4.7	6.8

[a] T: temperature, ρ: density, ΔH_{vap}: heat of vaporization, U_{pot}: potential energy, U_{self}: self-polarization energy, ϵ: static relative dielectric permittivity. [b] Reference 39. [c] Reference 54.

IV.2. The Use of the Charge-On-Spring Model in a QM/MM-pol Hamiltonian. After implementing the charge-on-spring model in the GROMOS96 code interfaced to ChemShell, we tested the variational character of the combined QM/MM-pol Hamiltonian by monitoring the convergence behavior of the 'electronic' energy of the system (energy of the QM electrons plus induced MM dipoles) for configurations taken every 100 steps from simulations for the separate reactants (rc = 0.4 nm) and the transition state (rc = 0.0 nm) in $\mathrm{DME_{pol}}$. We explicitly looked at the convergence of the total electronic energy, since the separate SCF procedures to solve for the QM electronic wavefunction or the positions of the MM charges-on-spring are strictly not variational due to their mutual influence. The QM, MM, and QM/MM energies were followed every QM-MM iteration step. It was found that both the QM electronic and MM self-polarization energy converged within 0.001 kJ $\mathrm{mol^{-1}}$ after 2 or 3 steps. No large fluctuations of the separate QM and MM energy terms were observed during the iterative process, indicating that the applied doubly iterative procedure is variational for the investigated system. The convergence

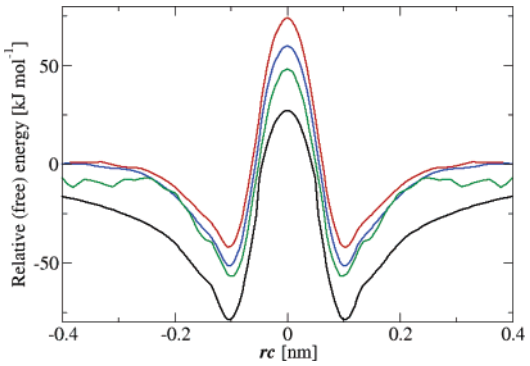

Figure 3. Gas-phase potential energy surface for the S_N2 reaction 3 along the reaction coordinate rc as defined in eq 17 at the PM3 level of theory (black line) and the corresponding free energy profile (green line) and the free energy profile for the same reaction in liquid dimethyl ether from QM/MM MD simulations using a nonpolarizable (blue line) and polarizable (red line) force field for the solvent. Values for the (free) energies are relative to the values for the separated reactants (corresponding with rc = ± 1.1 nm in the gas phase and rc = ± 0.4 nm in the condensed phase).

of the total 'electronic' energy of the system to within 0.002 kJ mol^{-1} is considered to be sufficient: the introduced inaccuracy is negligible in size when compared to the kinetic energy of the atomic degrees of freedom ($1/2\ k_BT$ = 1 kJ mol^{-1} at 248.15 K).

In our QM/MM-pol simulations, we did not observe artifacts due to the 'polarization catastrophe'.[31] That is, we did not see any induced MM dipole adopting infinitely large values due to close QM-MM van der Waals contacts and accordingly unrealistic large QM-MM contributions to the electric field. Apparently, the size of the van der Waals radii of the QM and MM nuclei was chosen large enough. Additionally, the large value for q_{pol} assures that displacements of the charges-on-spring from their adjacent polarizable center are small compared to the van der Waals radius of the atom, preventing the charges-on-spring to collapse onto the QM or other MM nuclei.

IV.3. The (Free) Energy Profiles for Reaction 3 in the Gas Phase and in Liquid DME. The gas-phase potential energy surface (PES) and the potentials of mean force (PMF) for reaction 3 in vacuum and in liquid dimethyl ether (DME) are presented in Figure 3. The PES and PMFs are given in the range of values for the reaction coordinate rc from −0.4 to 0.4 nm, whereas simulations were only performed at rc ≥ 0.0 nm. The symmetric profiles were obtained by mirroring the explicitly obtained part of the curves. Plotted values for the potential energy are relative to the value for the infinitely separated reactants, and free energies are relative to the value for which the PMF reaches a plateau.

The gas-phase formation energy of the reactant complex (RC) and transition state (TS) out of the reactants was found to be −79.0 kJ mol^{-1} and 26.9 kJ mol^{-1}, respectively. These values are in agreement with the values reported by Liu et al. (−18.9 kcal mol^{-1} and 6.4 kcal mol^{-1}, respectively)[5] and correspond with a clear picture of a double-well PES. Figure 3 shows that the calculation of the gas-phase PMF suffers from poor sampling in the dissociative regime(|rc| > 0.2 nm). Values for the restraining force are not converged in this regime, since the part of the phase space to be sampled increases due to a weakening of dipole-ion interactions between the separating reactants. Performing tenfold longer MC simulations at selected values for rc between 0.2 and 1.1 nm did not significantly improve convergence (results not shown). Thus, from the gas-phase MC simulations we could not estimate the plateau value for the separate reactants relative to the free energy values for smaller values of rc. Here it is obtained in an alternative way, via relative differences between the free energies of solvation ΔF_{solv} of the reactants Cl^-, NH_2Cl, and the TS in nonpolarizable DME. ΔF_{solv} was estimated at −109.6, −12.3 and −110.2 kJ mol^{-1}, respectively. Taking for X and Y in eq 4 the transition and reactant state, respectively, $\Delta\Delta F_{solv,XY}$ was estimated at 11.7 kJ mol^{-1}. Thus, the separated reactants are better solvated in DME, in accordance with Liu's findings discussed in section I. Using eqs 4 and 5 and a value of $\Delta F_{cond,XY} = 59.8$ kJ mol^{-1} (see Figure 3), the plateau value for the reactants in the gas phase is found to be 48.1 kJ mol^{-1} lower than the free energy of the transition state. An estimate of the errors in ΔF_{solv} is difficult to obtain when using the perturbation formula (eq 22). However, these errors do not contribute to $\Delta\Delta F_{solv}$ profiles along rc when calculated from eq 5, as is done in the next sections.

Figure 3 also presents the free energy profiles of reaction 3 in liquid DME obtained from our QM/MM simulations. These profiles have been corrected for the metric tensor effect (second term on the right of eq 20), which was found to contribute less than 1 kJ mol^{-1} to free energy differences along rc. Accumulated errors in the reactant complexation free energy and activation barrier were 6.0 and 7.3 kJ mol^{-1} for the simulations with the QM/MM-nonpol Hamiltonian (which employs the DME_{nonpol} force field) and 8.0 and 9.7 kJ mol^{-1} for the QM/MM-pol simulations, respectively, which are smaller than the corresponding free energy differences along rc and the relative differences with respect to the gas-phase potential energy values. To check for hysteresis, we redid the series of simulations in opposite direction (changing rc gradually from 0.4 to 0 nm). No noticeable differences between the PMFs for the different pathways were observed with maximum deviations in free energy differences along the reaction profile of 4 kJ mol^{-1}, which is within the estimated errors. Besides, we did not observe a solvent memory effect along the reaction coordinate, as indicated by the observed overlap of the radial distribution functions (rdf) of solvent molecules around the chlorides in the transition state and from a comparison of rdfs for the solvent molecules around the reactants (products) from simulations of the forward and backward reaction (results not shown). From these findings, we conclude that the simulation time and number of data points along the reaction coordinate are chosen sufficiently large to exclude hysteresis effects.

IV.4. The Effect of the Inclusion of Solvent Polarization Effects. Figure 3 shows that the inclusion of solvent electron polarization effects does not change the qualitative picture of a double-well free energy profile for reaction 3 in liquid DME, but the plateau value for the reactants is reached at a

smaller value for rc in the QM/MM-pol simulations than when using the DME_{nonpol} model. This indicates a stronger solvent screening by DME_{pol} of ion-dipole interactions between the separating reactants, in line with its larger dielectric permittivity (Table 2). Quantitative differences in the PMFs obtained from simulations using nonpolarizable or polarizable DME model are relatively small when compared to the change with respect to the PES in vacuum. However, when comparing the condensed-phase PMFs with the gas-phase *free* energy profile, solvent electron polarization effects are found to play a significant role in the change of the reaction profile upon solvation. Changes in the formation free energy of the TS and RC out of the separate reactants are much smaller upon solvation than when comparing the PMF in DME with the PES in vacuum. The increase in activation barrier when going from the gas-phase PES to the PMF in vacuum can be explained from the lower density of rotational and vibrational states of the classical S_N2 transition states, resulting in a loss of entropy upon complexation.[55] The loss in entropy upon RC and TS formation has a large effect on the gas-phase activation barrier and reduces the difference in activation barrier when going from the gas-phase simulations to the simulations using the DME_{nonpol} model to 11.7 kJ mol^{-1}. The increase in activation barrier when comparing the PMFs in vacuum and in DME_{pol} was estimated at 25.9 kJ mol^{-1}. Thus, we found a doubling of the solvent effect on the free energy barrier upon inclusion of solvent electron polarization effects.

Including solvent polarization effects does not substantially affect the properties of the QM subsystem along the reaction coordinate, such as the geometry of the substrates or its polarization by the solvent. When using either the nonpolarizable or polarizable solvent models, maximum differences of 0.002 nm for average bond distances in the reactive subsystem were observed (results not shown). Mulliken partial charges of the QM atoms along the reaction are shown in Figure 4a. Only in the range of rc = 0.02 nm to rc = 0.2 nm a small difference in polarization of the complex is found. In this regime, the attacking Cl^- has a slightly more negative charge (and the Cl more tightly bound to the nitrogen an accordingly more positive partial charge) in the QM/MM-pol simulations, probably due to solvent back polarization effects. This difference vanishes when going to the separated reactants (in which charge transfer from the NH_2Cl subunit to the chloride anion is not possible) or to the symmetric transition state.

In contrast, significant changes in the polarization of the solvent molecules are observed along rc. The localization of the QM subsystem's negative charge on the separate chloride anion leads to a stronger polarization of the solvent molecules in the reactant state. This is clearly indicated by trends in the total self-polarization energy U_{self} of the solvent. Figure 4b shows an increase of about 20 kJ mol^{-1} in U_{self} values when going from rc = 0.0 to 0.4 nm. Indeed, when comparing the transition and the reactant state we see a significant induction in the radial component of the average molecular dipole moment of the DME solvent molecules around the leaving chloride anion, see Figure 4c. In contrast,

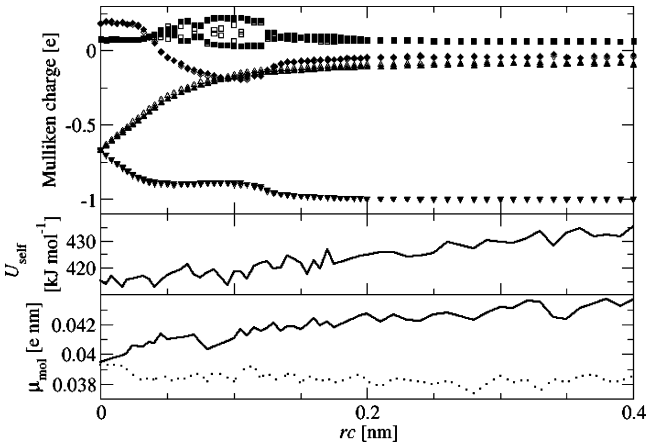

Figure 4. (a) Mulliken charges on atoms of the QM subsystem in liquid dimethyl ether along the reaction coordinate rc of reaction 3 as defined in eq 17, using the QM/MM-nonpol (closed symbols) and QM/MM-pol Hamiltonians (open symbols) (diamonds: nitrogen, squares: hydrogens, triangles up: chloride in NH_2Cl, triangles down: approaching or leaving chloride anion), (b) total self-polarization energy (in kJ mol^{-1}) of the solvent, and (c) radial component of the molecular dipole in the first solvation shell (radius = 0.6 nm) around the chlorides in the QM subsystem (approaching or leaving Cl^-: solid line, and Cl residing in NH_2Cl product/reactant: dotted line) along rc for reaction 3 in liquid dimethyl ether, in simulations using the QM/MM-pol Hamiltonian.

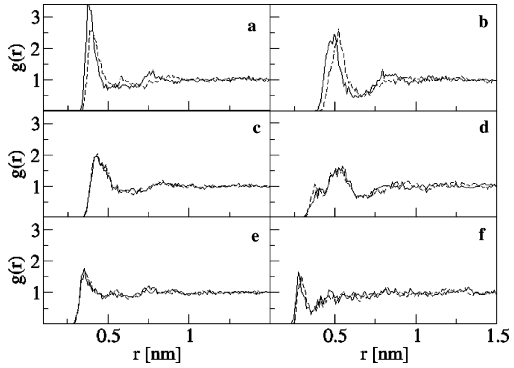

Figure 5. Radial distribution functions of solvent atoms (C, O) around QM solute atoms (Cl^-, Cl, N) for the separated reactants of reaction 3 (corresponding with a value for the reaction coordinate rc as defined in eq 17 of 0.4 nm) in liquid dimethyl ether from simulations using the QM/MM-nonpol (dashed lines) and the QM/MM-pol (solid lines) Hamiltonians: (a) Cl^-−C, (b) Cl^-−O (c) Cl−C, (d) Cl−O, (e) N−C, and (f) N−O atom pairs.

this value only moderately decreases for the DMEs around the chloride atom that remains attached to N.

The stronger induction of the MM molecular dipoles in the reaction state leads to a better solvation of the Cl^- anion by the polarizable solvent, when compared to the simulations using the nonpolarizable force field. Figure 5a shows an increase in the first peak of the radial distribution function (rdf) of the carbon of DME around the Cl^- upon inclusion of solvent polarization effects in the Hamiltonian. Additionally, the peak slightly shifts to the left, hinting at a closer approach of the DME molecules. This is even more strongly indicated by the shift in the first peak in the Cl^-−O rdf

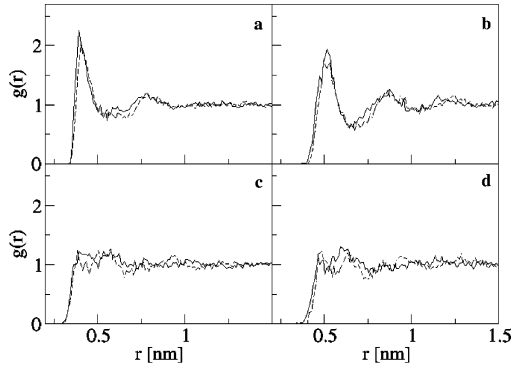

Figure 6. Radial distribution functions of solvent atoms (C, O) around QM solute atoms (Cl, N) for the transition state of reaction 3 (corresponding with a value for the reaction coordinate rc as defined in eq 17 of 0.0 nm) in liquid dimethyl ether from simulations using the QM/MM-nonpol (dashed line) and the QM/MM-pol (solid line) Hamiltonians: (a) Cl−C, (b) Cl−O, (c) N−C, and (d) N−O atom pairs.

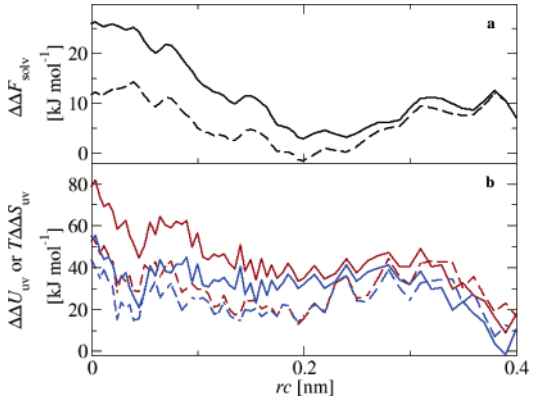

Figure 7. (a) Free energy of solvation relative to the reactants at infinite separation ($\Delta\Delta F_{solv}$) and (b) the corresponding differences in the solute−solvent interaction energy ($\Delta\Delta U_{uv}$, red lines) and solute−solvent entropy ($T\Delta\Delta S_{uv}$, blue lines) of the reactive subsystem along the reaction coordinate rc as defined in eq 17 for reaction 3 in liquid dimethyl ether from simulations using a QM/MM-nonpol (dashed lines) and QM/MM-pol (solid lines) Hamiltonian. $\Delta\Delta F_{solv}$, $\Delta\Delta U_{uv}$, and $T\Delta\Delta S_{uv}$ were calculated using eqs 5 and 10−13.

(Figure 5b). The difference in shift of the first peaks in the Cl^-−C and Cl^-−O rdfs hints at a difference in orientation of the polarizable DME molecules around the chloride anion compared to the DME_{nonpol} molecules. However, this could not be unambiguously confirmed from a comparison of the Cl^-−C−O angle involving carbons in the first solvation shell around the ion: only a small difference was found in the simulations using DME_{nonpol} and DME_{pol} with values of 123.6 and 125.6 degrees, respectively. The solvent structure around the neutral NH_2Cl substrate is hardly affected upon inclusion of solvent polarization, as shown by the similar shape of the radial distribution functions shown in Figure 5c−f. From the rdfs of the solute−solvent atom pairs for the TS (see Figure 6) we see a slight improvement of TS solvation upon using a polarizable DME force field, as reflected by the small shifts to the left in the first solvation peaks for the Cl−C, Cl−O, and N−O rdfs (Figure 6a,b,d). However, these changes are much smaller than the increase in and shift of the first peak in the Cl^-−C and Cl^-−O rdfs for the separate anion (Figure 5a,b). Thus, inclusion of solvent polarization effects leads to a further improvement of the solvation of the charge-separated reactants when compared to the transition state. Together with the enhancement of the dipole of the solvent molecules around the chloride ion making energetic interactions stronger than in the TS, this causes an increase in the activation barrier of reaction 3 in DME when going from a nonpolarizable to a polarizable description of the solvent.

IV.5. An Energy-Entropy Decomposition of the Relative "Free Energy of Solvation" of the QM Subsystem. Figure 7a shows the differences in the free energy of solvation of the QM subsystem along the reaction coordinate relative to the reactants at infinite separation ($\Delta\Delta F_{solv}$) in polarizable and nonpolarizable DME, as calculated from Figure 3 using eq 5. This profile quantitatively shows that the separated reactants are better solvated than the reactant complex and transition state (values for $\Delta\Delta F_{solv}$ are positive over the whole range of rc values) and that this effect is more pronounced in DME_{pol} (values for $\Delta\Delta F_{solv}$ being more positive). Values for $\Delta\Delta F_{solv}$ along rc were decomposed into differences in the energetic ($\Delta\Delta U_{uv}$) and entropic ($T\Delta\Delta S_{uv}$) interactions between the solute (QM) and solvent (MM) subsystems relative to the reactants at infinite separation, see Figure 7b. Errors in $\Delta\Delta U_{uv}$ were estimated as the sum in the errors of the separate terms in eqs 10 or 12 and sum up to 2−3 kJ mol^{-1}.

From Figure 7b, it can be seen that values for the solute−solvent interaction energy with respect to the separate reactants increase in going to the reactant complex and transition state. The trend in $\Delta\Delta U_{uv}$ being positive over the whole range of rc is counteracted by a gain in entropy upon going to rc = 0.0 nm which (from Figures 5 and 6) can be understood in terms of a loss in solvent structure compared to the reactant state. However, the trend in solute−solvent entropy only partly counteracts the one in $\Delta\Delta U_{uv}$, resulting in $\Delta\Delta F_{solv}$ being positive over the whole range of rc. This is a quantitative measure of the solute−solvent interaction *energy* determining the increase in activation free energy upon solvation.

From Figure 7b, the solute−solvent interaction energy also determines the further increase in activation barrier and RC formation free energy when going from the nonpolarizable to the polarizable DME solvent. In the QM/MM-pol simulations, $\Delta\Delta U_{uv}$ is more positive when rc approaches zero (in line with the simultaneous decrease in U_{self}, see Figure 4b), again only partly counteracted by a further increase in entropy at rc going to zero (which can be explained from the change in the first peak in the Cl^-−C and Cl^-−O rdfs when going from the QM/MM-nonpol to the QM/MM-pol simulations, see Figure 5).

Finally, we shortly comment on the use of an atomistic representation of the solvent based on our results. First of all, the use of a continuum-electrostatic model in the gas-phase MC simulations to account for solvent effects in a mean-field manner might yield a condensed-phase PMF similar in shape to the ones obtained in our more expensive QM/MM-(non)pol simulations. However, these simulations

can of course not capture the change of the solvent structure around the QM subsystem (as reflected by Figures 5 and 6) or the change in $Cl^- - C_{DME} - O_{DME}$ angle involving DME's carbon in the first solvation shell of the anion (from about 120 to 160 degrees) when going from the reactant to the transition state. Similarly, one may try to correct for the missing solvent electronic polarization effects in the QM/MM-nonpol simulations in an average way, by including the energetic contribution of the polarization of the MM atoms via linear-response theory. This would be less expensive than using the iterative QM/MM-pol approach. However, only in the latter case one can observe changes in the microscopic structure around the reactive subsystem induced by the polarization of the solvent, such as the improved solvation of the Cl^- anion (see Figure 5a,b).

V. Conclusions

In the present work, we repeated a combined QM/MM MD simulation study[5] on the free energy profile of reaction 3 in liquid dimethyl ether (DME). Additionally, we performed the same set of simulations in which electronic polarization of the solvent was explicitly taken into account using the charge-on-spring (COS) model with the aim of analyzing explicit solvent polarization effects upon the reaction. For this purpose, a COS-based force field for DME was parametrized based on the nonpolarizable parameter set used, and the COS model was implemented into the GROMOS interface to ChemShell using a doubly iterative scheme. The combined Hamiltonian for reaction 3 in polarizable DME was found to behave variationally: under the chosen settings, total energies converge within a few iteration steps. No occurrence of the polarization catastrophe was observed.

Including solvent electronic polarization effects does not change the qualitative picture of the double-well free energy profile of reaction 3 in DME. However, the higher dielectric permittivity of the polarizable solvent results in stronger solvent screening of the interactions between the separated reactants, resulting in a plateau value for the free energy corresponding to the separated reactants at a smaller value of rc than in the simulations using the nonpolarizable DME_{nonpol} force field. Moreover, when compared to the gas-phase potential of mean force (PMF), we find a doubling of the change in activation free energy upon solvation when comparing its value from the simulations using the DME_{nonpol} model with those from the QM/MM-pol simulations. This could be explained from a stronger polarization of the polarizable solvent molecules around the reactants than those surrounding the transition state in which the net-charge of the reactive subsystem is more smeared out. This leads not only to stronger QM-MM electrostatic interactions for large rc values but also to a better solvation of the Cl^- anion when compared to the simulations in DME_{nonpol}. The origin of the increase in activation barrier upon solvation and upon explicit inclusion of solvent polarization can be understood from a quantitative energy-entropy decomposition of the solute−solvent interactions. According to this analysis, solvent (polarization) effects on the PMF of reaction 3 in DME are driven by changes in the solute−solvent interaction energy along rc, which are only partly counteracted by the solute−solvent entropy increase upon loss in solvent structure when going from the reactant to the transition state.

Acknowledgment. The authors want to thank Dirk Bakowies, Salomon Billeter, and Haiyan Liu for stimulating discussions. Financial support from the Max-Planck Gesellschaft, from the National Center of Competence in Research (NCCR) in Structural Biology, and from grant number 200021-109227 of the Swiss National Science Foundation is gratefully acknowledged.

References

(1) Warshel, A.; Levitt, M. *J. Mol. Biol.* **1976**, *103*, 227.

(2) Warshel, A. *Computer Modeling of Chemical Reactions in Enzymes and Solutions*; John Wiley: New York, 1991.

(3) Senn, H. M.; Thiel, W. *Top. Curr. Chem.* **2007**, *268*, 173.

(4) Lin, H.; Truhlar, D. G. *Theor. Chim. Acc.* **2007**, *117*, 185.

(5) Liu, H. Y.; Müller-Plathe, F.; van Gunsteren, W. F. *Chem. Eur. J.* **1996**, *2*, 191.

(6) Singh, U. C.; Kollman, P. A. *J. Comput. Chem.* **1986**, *7*, 718.

(7) Field, M. J.; Bash, P. A.; Karplus, M. *J. Comput. Chem.* **1990**, *11*, 700.

(8) Sherwood, P.; de Vries, A. H.; Guest, M. F.; Schreckenbach, G.; Catlow, C. R. A.; French, S. A.; Sokol, A. A.; Bromley, S. T.; Thiel, W.; Turner, A. J.; Billeter, S.; Terstegen, F.; Thiel, S.; Kendrick, J.; Rogers, S. C.; Casci, J.; Watson, M.; King, F.; Karlsen, E.; Sjovoll, M.; Fahmi, A.; Schafer, A.; Lennartz, C. *J. Mol. Struct.* (*Theochem*) **2003**, *632*, 1.

(9) Glukhovtsev, M. N.; Pross, A.; Radom, L. *J. Am. Chem. Soc.* **1995**, *117*, 9012.

(10) Thompson, M. A.; Schenter, G. K. *J. Phys. Chem.* **1995**, *99*, 6374.

(11) Thompson, M. A. *J. Phys. Chem.* **1996**, *100*, 14492.

(12) Bryce, R. A.; Buesnel, R.; Hillier, I. H.; Burton, N. A. *Chem. Phys. Lett.* **1997**, *279*, 367.

(13) Field, M. J. *Mol. Phys.* **1997**, *91*, 835.

(14) Dupuis, M.; Aida, M.; Kawashima, Y.; Hirao, K. *J. Chem. Phys.* **2002**, *117*, 1242.

(15) Vesely, F. J. *J. Comput. Phys.* **1977**, *24*, 361.

(16) van Belle, D.; Couplet, I.; Prevost, M.; Wodak, S. J. *J. Mol. Biol.* **1987**, *198*, 721.

(17) Rappe, A. K.; Goddard, W. A. *J. Phys. Chem.* **1991**, *95*, 3358.

(18) Rick, S. W.; Stuart, S. J.; Berne, B. J. *J. Chem. Phys.* **1994**, *101*, 6141.

(19) Drude, P. *The Theory of Optics*; Longmans, Green, and Co.: New York, 1902.

(20) Born, M.; Huang, K. *Dynamic Theory of Crystal Lattices*; Oxford University Press: Oxford, UK, 1954.

(21) Straatsma, T. P.; McCammon, J. A. *Mol. Simul.* **1990**, *5*, 181.

(22) Yu, H. B.; Hansson, T.; van Gunsteren, W. F. *J. Chem. Phys.* **2003**, *118*, 221.

(23) van Gunsteren, W. F.; Billeter, S. R.; Eising, A. A.; Hünenberger, P. H.; Krüger, P.; Mark, A. E.; Scott, W. R. P.; Tironi, I. G. *Biomolecular Simulation: The GROMOS96 Manual and User Guide*; vdf Hochschulverlag: ETH Zürich, Switzerland, 1996.

(24) Scott, W. R. P.; Hünenberger, P. H.; Tironi, I. G.; Mark, A. E.; Billeter, S. R.; Fennen, J.; Torda, A. E.; Huber, T.; Krüger, P.; van Gunsteren, W. F. *J. Phys. Chem. A* **1999**, *103*, 3596.

(25) van der Vegt, N. F. A.; van Gunsteren, W. F. *J. Phys. Chem. B* **2004**, *108*, 1056.

(26) van der Vegt, N. F. A.; Trzesniak, D.; Kasumaj, B.; van Gunsteren, W. F. *Chem. Phys. Chem.* **2004**, *5*, 144.

(27) Trzesniak, D.; van der Vegt, N. F. A.; van Gunsteren, W. F. *Phys. Chem. Chem. Phys.* **2004**, *6*, 697.

(28) Lee, M. E.; van der Vegt, N. F. A. *J. Am. Chem. Soc.* **2006**, *128*, 4948.

(29) van der Vegt, N. F. A.; Lee, M. E.; Trzesniak, D.; van Gunsteren, W. F. *J. Phys. Chem. B* **2006**, *110*, 12852.

(30) Yu, H. A.; Karplus, M. *J. Chem. Phys.* **1988**, *89*, 2366.

(31) Yu, H. B.; van Gunsteren, W. F. *Comput. Phys. Commun.* **2005**, *172*, 69.

(32) Berendsen, H. J. C.; Grigera, J. R.; Straatsma, T. P. *J. Phys. Chem.* **1987**, *91*, 6269.

(33) Billeter, S. R.; Turner, A. J.; Thiel, W. *Phys. Chem. Chem. Phys.* **2000**, *2*, 2177.

(34) Thiel, W. *MNDO99*, V 6.1 ed.; Max-Planck-Institut für Kohlenforschung: Mülheim an der Ruhr, Germany, 2003.

(35) Miller, K. J. *J. Am. Chem. Soc.* **1990**, *112*, 8533.

(36) Berendsen, H. J. C.; Postma, J. P. M.; van Gunsteren, W. F.; DiNola, A.; Haak, J. R. *J. Chem. Phys.* **1984**, *81*, 3684.

(37) Ryckaert, J. P.; Ciccotti, G.; Berendsen, H. J. C. *J. Comput. Phys.* **1977**, *23*, 327.

(38) Tironi, I. G.; Sperb, R.; Smith, P. E.; van Gunsteren, W. F. *J. Chem. Phys.* **1995**, *102*, 5451.

(39) Maass, O.; Booner, E. H. *J. Am. Chem. Soc.* **1922**, *44*, 1709.

(40) Neumann, M. *Mol. Phys.* **1983**, *50*, 841.

(41) Senn, H. M.; Thiel, S.; Thiel, W. *J. Chem. Theory Comput.* **2005**, *1*, 494.

(42) Beveridge, D. L.; DiCapua, F. M. *Annu. Rev. Biophys. Biophys. Chem.* **1989**, *18*, 431.

(43) Carter, E. A.; Ciccotti, G.; Hynes, J. T.; Kapral, R. *Chem. Phys. Lett.* **1989**, *156*, 472.

(44) Ciccotti, G.; Ferrario, M.; Hynes, J. T.; Kapral, R. *Chem. Phys.* **1989**, *129*, 241.

(45) Paci, E.; Ciccotti, G.; Ferrario, M.; Kapral, R. *Chem. Phys. Lett.* **1991**, *176*, 581.

(46) Billeter, S. R.; van Gunsteren, W. F. *J. Phys. Chem. A* **2000**, *104*, 3276.

(47) Sprik, M.; Ciccotti, G. *J. Chem. Phys.* **1998**, *109*, 7737.

(48) den Otter, W. K.; Briels, W. J. *J. Chem. Phys.* **1998**, *109*, 4139.

(49) Schlitter, J.; Klahn, M. *J. Chem. Phys.* **2003**, *118*, 2057.

(50) Schlitter, J.; Klahn, M. *Mol. Phys.* **2003**, *101*, 3439.

(51) Trzesniak, D.; Kunz, A. P. E.; van Gunsteren, W. F. *Chem. Phys. Chem.* **2007**, *8*, 162.

(52) Allen, M. P.; Tildesley, D. J. *Computer Simulation of Liquids*; Oxford University Press: New York, 1987.

(53) Zwanzig, R. W. *J. Chem. Phys.* **1954**, *22*, 1420.

(54) Kennedy, R. M.; Sagenkahn, M.; Aston, J. G. *J. Am. Chem. Soc.* **1941**, *63*, 2267.

(55) Olmstead, W. N.; Brauman, J. I. *J. Am. Chem. Soc.* **1977**, *99*, 4219.

CT7000123